LAND SUBSIDENCE MODELING BY ADVANCED D-InSAR TECHNIQUES

Thesis submitted to the Andhra University, Visakhapatnam in partial fulfillment of the requirement for the award of

Master of Technology in Remote Sensing and GIS

Submitted By

SIDDHARTHA BHAUMICK

Supervised By

Dr. R. S. CHATTERJEE
Scientist / Engineer-'SF'

Geosciences and Geo-hazards Department
Indian Institute of Remote Sensing, ISRO
Dept. of Space, Govt. of India
Dehradun – 248 001, India

August, 2013

CERTIFICATE

This is to certify that the project entitled **"LAND SUBSIDENCE MODELING BY ADVANCED D-InSAR TECHNIQUES"** is a bonafide record of work carried out by **Mr. Siddhartha Bhaumick**. The report has been submitted in partial fulfillment of requirement for the award of Master of Technology in Remote Sensing and GIS in Natural Resource Management with specialisation in Geosciences, conducted at Indian Institute of Remote Sensing, Dehradun, during 23 Aug 2011 to 16 Aug 2013. The work has been carried out under the supervision of **Dr. R. S. Chatterjee, Scientist / Engineer 'SF'**, Geosciences and Geohazards Department.

Dr. P.K. Champati ray
Scientist 'SG'
Head, Geosciences and Geohazards Department

Dr. R. S. Chatterjee
Scientist / Engineer 'SF'
Geosciences and Geohazards Department

Dr. Y. V. N. Krishnamurthy
Director
IIRS, Dehradun

Dr. S.K. Saha
Dean (Academics)
IIRS, Dehradun

DEDICATED TO MY LOVING PARENTS

ABSTRACT

Differential Interferometric Synthetic Aperture Radar (D-InSAR) is a microwave remote sensing technique for measuring spatially continuous surface deformation at high precision. Land Subsidence is the motion of a surface (Earth's surface) as it shifts downward relative to a datum such as sea level. Research studies have shown that there are several approaches aimed at D-InSAR time series generation, but this study explores the feasibility of EMD (Empirical Mode Decomposition) for deformation modeling and comparative analysis of the results with D-InSAR. Jharia coalfields, India which has been experiencing subsidence for several decades due to underground mining and coal fire was taken as the study area. In this work, 8 high resolution single polarization (FBS) modes ALOS PALSAR datasets acquired during 2007-2010 were used. Merged SRTM (Shuttle Radar Topographic Mission) and CARTOSAT Digital Elevation Model (DEM) was used for removal of topography. Among 28 differential interferograms generated, 10 good interferograms were chosen because in these 10 pairs not only well defined subsidence fringes were obtained, but also most of the fringes are overlapping which denotes continuous subsiding areas. The fringe areas were integrated to obtain the total subsidence affected areas during the observation period with rate of subsidence. The maximum subsidence rate calculated through D-InSAR processing is 35.235cm/year and minimum is 17.62cm/year. EMD basically decomposes an image into narrow band oscillatory components called IMF and a residue which is monotonic. In this study, EMD was applied on stack of unwrapped interferograms at each pixel where subsidence fringes are present, and the reconstructed D-InSAR time series was used for further analysis. IMF corresponds to non-linear deformation and residue corresponds to linear deformation. So for each fringe area statistics of IMF and residue was calculated and compared with the results obtained from D-InSAR. After that subsidence generated from D-InSAR and EMD are validated with respect to spatial extent and field evidences. Most of the subsidence fringes were in the eastern parts of the coalfield, but some are in the south-eastern and north-western part of the study area. Deformation modeling through EMD is similar to SBAS (Small Baseline Subset) approach, but SBAS cannot be applied in this work because of limited number of datasets.

Keywords: D-InSAR, land subsidence, EMD, SBAS, IMF, residue, fringes, DEM, monotonic.

ACKNOWLEDGEMENTS

All glory and honor be to the Almighty God, who showered His generous grace.

Firstly, I would like to express my deepest gratitude to my parents for their unfailing humor, warm wishes and their endless support and love which helped me to sail the boat against the gusty winds.

I wish to give special thanks to Dr. Y. V. N. Krishnamurthy (Director, IIRS) & Dr. S. K. Saha, Group Director, Earth Resources and System Studies Group and Dean (Academics) for allowing me to carry out this project work and also for their kind support and facilities they had provided me throughout the project work.

I express my sincere regards to my supervisor Dr. R. S. Chatterjee who stood as a backbone throughout my research period. Without his constant support, guidance and encouragement, the completion of this research work would not have been possible. I am very grateful to him for having given me an opportunity to work as his student and for sharing his immense knowledge with me.

I would like to express my sincere gratitude to Dr. P. K. Champati Ray (Head, Geosciences Division) for his encouragement and support.

My thanks are also to other faculty members and staff of the department who had directly or indirectly helped me in course of time.

I would also take the opportunity for giving my sincere and humble thanks to the officers of BCCL who helped me by providing useful data and necessary support regarding the field.

I would like to thanks to my friends specially Sivi, Shankar, Surya and Sai Bhardwaj for their moral and technical support throughout my project work.

This acknowledgement cannot be complete without expressing my very special thanks to my unforgettable friend Y. Benthungo Murry for his continuous help, support, cooperation and encouragement throughout the M. Tech. program.

Siddhartha Bhaumick
(সিদ্ধার্থ ভৌমিক)

TABLE OF CONTENTS

LIST OF FIGURES

LIST OF TABLES

1. INTRODUCTION

1.1. Background

Advancements in science and technology have led to the application of Remote Sensing and GIS (Geographic Information System) in the field of topographic measurements. The science of remote sensing deals with collection of images of features on the earth's surface without having any physical contact with the objects. The exploitation of electromagnetic spectrum including microwaves has led to remarkable inventions such as radio, television, mobile communication, microwave ovens and RADAR (Radio Detection and Ranging) system (Woodhouse, 2006). The development in the field of microwave remote sensing has helped to shape the models of today's world.

Imaging of the earth surface can be done by RAR (Real Aperture Radar) systems but the resolution is limited by power and size of the footprint of the RADAR beam which in itself is based on the aperture size, and thus RAR systems are used only for few remote sensing applications (Burgmann, et al., 2000). This limitation in providing the useful spatial resolution is overcome by SAR (Synthetic Aperture Radar) systems. In case of SAR system, a large antenna is synthesized by means of offline processing techniques which use the Doppler Effect in the acquired data. SAR uses the techniques of signal processing and satellite orbital information which thereby provides a much higher resolution RADAR image in range and azimuth directions as compared to RAR systems.

In recent times, topographic data is generated using many techniques. Topographic data generation involves stereographic techniques using optical remote sensing and lately with evolution of GPS (Global Positioning System) technology, point positioning has come to light (Hanssen, 2001). Among the techniques, RADAR interferometry is not only used for detection and ranging but also for imaging the Earth's surface, as such it is a very promising technique for accurate deformation measurements. Recently with the increase in number of SAR (Synthetic Aperture Radar) sensors on different space borne platforms, these sensors are able to collect data all over the earth (Hanssen, 2001). SAR operational wavelength ranging from 1mm to 1m is an additional advantage of penetration through clouds, haze, dust (but not through heavy rainfalls) because the longer wavelengths are not susceptible to atmospheric scattering, which affects shorter optical wavelengths (Hanssen, 2001).

RADAR imaging through SAR systems using InSAR (Interferometric Synthetic Aperture Radar) and D-InSAR (Differential Interferometric Synthetic Aperture Radar) are the widely used tools for measuring topographic profile and surface deformations (Rosen, et al., 2000).

1.2. Motivation and problem statement

D-InSAR is a powerful remote sensing technique for measuring topographic profile and spatially continuous surface deformation at high precision. Studies have been conducted for several approaches aimed at D-InSAR time series generation, but in this work the main focus is on deformation modeling i.e. separation of linear and non-linear deformation by EMD (Empirical Mode Decomposition). It is totally adaptive and data driven approach and is suitable for analyzing non-linear and non-stationary time series data.

In this work, trend analysis will be done by statistical trend test approach because statistical trend tests provide a more appropriate way to describe trends in long time series than linear regression. Studies have been conducted that primary testing of trends in residue obtained by EMD of D-InSAR time series was done by non-parametric Mann-Kendall test because it gives the strength and direction of trend but not its magnitude. Hence, Sen's slope estimator will be used to find the slope of the trend.

This research aims to explore the feasibility of EMD for deformation modeling and comparative analysis of the results with D-InSAR.

1.3. Research identification

To arrive at a solution for the problem statement mentioned in section 1.2, the scientific objectives and research questions are framed below to derive the solution.

1.3.1. Scientific objectives

- Delineation of subsiding areas and calculation of rate of subsidence.
- Modeling of deformation time series by Empirical Mode Decomposition technique.

1.3.2. Research questions

- How far L-band data is suitable for detecting surface deformation areas?
- How far EMD is suitable for deciphering deformation history?

2. LITERATURE REVIEW

2.1. D-InSAR

Differential Interferometric Synthetic Aperture Radar (D-InSAR) is a microwave remote sensing technique that allows us to investigate surface deformation phenomena with centimeter to millimeter accuracy and with a large spatial coverage capacity (Gabriel, et al., 1989). In particular, the D-InSAR technique exploits the phase difference, often referred to as interferogram, between two SAR images relevant to temporally separated observations of an investigated area and provides a measurement of the ground deformation projection along the Radar Line Of Sight (LOS).

The principle of D-InSAR is:-

- Interference of phase of two or more SAR acquisitions over the same area.
- Measures phase difference and translate to path difference between different SAR acquisitions.
- Obtain surface deformation from path difference at high precision.

The phase difference of a repeat-pass InSAR ($\Delta\Phi$) can be obtained by combining 2 complex SAR images (Chatterjee, et al., 2006). Therefore,

$$\Delta\psi_{int} = \Delta\psi_{flat} + \Delta\psi_{topo} + \Delta\psi_{mov} + \Delta\psi_{atmos} + \Delta\psi_{noise} \pm n * 2\pi \quad (2.1)$$

where,

$\Delta\psi_{flat}$ = flat earth component related to range distance differences in absence of topography.

$\Delta\psi_{topo}$ = topographic phase.

$\Delta\psi_{mov}$ = phase contribution due to ground displacement occurring between 2 SAR image acquisitions.

$\Delta\psi_{atmos}$ = phase component due to atmospheric disturbances.

$\Delta\psi_{noise}$= phase due to decorrelation noise.

In the term, $n * 2\pi$, n is a whole number, viz., 1, 2, 3,…including 0 and represents the number of phase cycles in the wrapped phase difference (Chatterjee, et al., 2006).

More analytically $\Delta\psi_{flat}$ is assumed to be known, and $\Delta\psi_{topo}$ can be extracted from an external DEM. Differential RADAR interferometry which is a result of the phase difference of two SAR images is a combination of two approaches: motion sensitivity and sensitivity to topography as given by a sensor temporal change and sensor location change respectively. DInSAR started gaining recognition due to its deformation mapping capability.

2.2. Land subsidence

Land Subsidence is the motion of a surface (Earth's surface) as it shifts downward relative to a datum such as sea level. It is a gradual settling or sudden sinking of the Earth's surface due to movement of earth materials. It can be induced from mining, ground water and oil and gas extraction. The opposite of subsidence is uplifting which results in an increase in elevation.

2.2.1. Causes of land subsidence

Active underground mining and subsurface coal fire are the main causes of land subsidence. Additionally, subsidence can occur at any time over old mine workings, regardless how long it has been deserted due to the existence of voids and weak supporting pillars (Lokhande, et al., 2009). The duration of subsidence resulting from mining consists of two phases a.) Active and b.) Residual (Lokhande, et al., 2009). Active subsidence refers to all movements occurring simultaneously with the mining operations, while residual subsidence is that part of the surface deformation that occurs following the cessation of mining (Lokhande, et al., 2009). Subsidence in old workings causes severe damage to surface structures. Jharia coalfield is facing subsidence problems due to the presence of old workings which are generally waterlogged and about a dozen of them have subsided in recent past causing severe damages to surface topography and also further subsidence are caused due to coal fires which leads to degradation of surface land and environment.

2.2.2. Impacts of land subsidence

Impacts of subsidence over different categories are given below:-

- Subsidence upto about 500mm were not visually felt in barren areas (Saxena, 1991).
- Subsidence upto a magnitude of about 650mm over hydraulically sand stowed workings did not cause any visual distortion in surface topography or impact on surface vegetation (Saxena, 1991).
- Subsidence over unapproachable workings also causes discontinuities and pot holes (Saxena, 1991).
- The width of cracks on the surface varies and the maximum subsidence observed was over 1000mm due to extraction of 8m thick seam at a depth of about 70m (Saxena, 1991).
- In general the impact of subsidence on surface topography was very prominent over caved workings at shallow to very shallow depths (Saxena, 1991).
- Subsidence of magnitude 600mm cause severe disturbances in sub-surface and underground water regime resulting in loss of water from aquifers and water tables (Saxena, 1991).
- Subsidence with cracks retards vegetation growth on the surface due to loss of water from top-soil (Saxena, 1991).
- At central portion of subsided areas water logging were seen very commonly.

- Subsidence were generally sudden over unapproachable old workings and also over current workings at depths upto about 100m (Saxena, 1991).
- Damage to buildings took place even with subsidence as low as 300-500mm over workings at a depth of about 300m (Saxena, 1991).

2.2.3. Remedial measures taken by the mining agencies

In old and abandoned mines underground workings are not approachable. Hence, there are limited approaches to prevent the intensity of subsidence, but there are few techniques to avoid further subsidence depending upon the causes of land subsidence (Lokhande, et al., 2009).

- **Fire**: Fires can be dealt by surface sealing, inundation and remote sealing (Bannerjee, 1985).
- **Void filling**: Point support method and areal backfilling are the two widely used methods for filling old underground voids (Lokhande, et al., 2009).
- **Cracks**: Surface cracks should be filled with soil to avoid inflow of water which may lead to pot-holes as well as washing out of underground filing materials (Lokhande, et al., 2009).
- **Sealing of mine entrance**: BCCL (Bharat Coking Coal Limited) and CIL (Coal India Limited) were stopping the illegal mining operation and robbing of pillars by local people, from old and abandoned workings by sealing the mine entries.
- **Water**: De-watering of old workings should be avoided if surface structures exists on it (Lokhande, et al., 2009).

2.3. Study of advanced D-InSAR techniques

2.3.1. PS (Persistent Scatterers)

Persistent Scatterer Interferometry (PSI) technique was developed by Ferretti in 1999. PSI and StaMPS (Standard Method for Persistent Scatterer) approach helps us to measure deformation with uncertainties of one millimeter per year, interpreting time-series of interferometric phases at coherent point scatterers (Ruiz, et al., 2008). This technique is very useful for analysis of urban areas, where angular structures produce efficient reflectors that dominate background scattering.

The PS method uses large stacks of images to generate differential interferograms with respect to one common master. The PSI approach relies on identifying pixels whose scattering properties vary little with time and look angle (Ferretti, et al., 1999, 2000, 2001). Pixels that are dominated by a singular scatterer best meet this criteria; therefore images are processed at full resolution to increase the chance of being only one dominant scatterer present, and also to reduce the contribution from other scatterers within each pixel (Ruiz, et al., 2008). In images where most pixels contain multiple scatterers of similar strength, PS

approach is less optimal because scattering characteristics of these pixels vary substantially with look angle.

Although PS-InSAR deformation measurements may be very precise, but the limitation is that it does not necessarily imply a reliable estimation of the parameters of interest – the various deformation regimes. PS-InSAR deformation measurements may be caused by different types of deformation such as gas extraction, shallow compaction or structural instabilities making unambiguous interpretation very difficult (Ferretti, et al., 2001).

2.3.2. SBAS (Small Baseline Subset)

The SBAS technique is a D-InSAR approach that allows us to detect Earth's surface deformation and also to analyze their temporal evolution. It relies on the use of small baseline differential SAR interferograms and on the application of Singular Value Decomposition (SVD) method to link independent SAR acquisition data set, separated by large baselines, thus increasing the number of data used for the analysis.

The algorithm first implements a selection of the coherent pixels in which the noise effects can be assumed negligible. On these pixels decoupling of the deformation signal component from undesired patterns, referred to as topographic and atmospheric artifacts, is carried out by exploiting the characteristics of these patterns. In particular, the interferometric phase component relevant to the topographic artifacts is correlated with the vector of the spatial baselines of the interferograms sequence; moreover the atmospheric phase signals are highly correlated in the space but poorly in time (Ferretti, et al., 2000). Based on these characteristics, the SBAS technique performs an estimation of these undesired signals that are subsequently filtered out from the measured interferometric phase, finally leads to the generation of deformation time series.

A detailed discussion on SBAS approach can be found in (Berardino, et al., 2002), but accordingly we are highlighting some of the key issues of the algorithm.

Considering N + 1 SAR images relative to the same area, acquired at the chronologically ordered times (t_0, ……., t_N); assuming that each acquisition may be combined with at least one other image and also assuming that all the images are co-registered with respect to master image that allows us to identify a common spatial grid. The starting point of the SBAS technique is represented by the generation of a number, say M, of multilooked D-InSAR interferograms that involves the previously mentioned set of N + 1 SAR acquisitions. Also note that each of these interferograms should be calibrated with respect to a single pixel located in an area that can be assumed stable or, at least, with known deformation behavior; this point is referred to as reference SAR pixel.

Now considering a generic pixel of azimuth and range coordinates (x, r); the expression of the generic j-th interferogram ($j = 1, \dots\dots\dots\dots, M$) computed from the SAR acquisitions at times t_A and t_B , will be the following (Tizzani, et al., 2007).

$$\begin{aligned}\delta\phi_j(x,r) &= \phi(t_B,x,r) - \phi(t_A,x,r) \\ &\approx \frac{4\pi}{\lambda}[d(t_B,x,r) - d(t_A,x,r)]\end{aligned} \tag{2.2}$$

And

$$\phi(t_i,x,r) = \frac{4\pi}{\lambda} d(t_i,x,r) \tag{2.3}$$

$$d(t_0,x,r) = 0 \tag{2.4}$$

where λ is the radar wavelength, $\phi(t_i,x,r)$ is the unknown phase of the image involved in the interferogram generated between the time t_0 and t_i , $d(t_A,x,r)$ and $d(t_B,x,r)$ are the radar line of sight (LOS) projections of the cumulative surface deformation at the two times t_A and t_B.

In order to get a physically sound solution, replace the unknowns with the mean phase velocity between time-adjacent acquisitions, then the new unknowns become:

$$v = \left[v_1 = \frac{\phi(t_1,x,r)}{t_1 - t_0}, \dots\dots\dots, v_N = \frac{\phi(t_N,x,r) - \phi(t_{N-1},x,r)}{t_N - t_{N-1}}\right] \tag{2.5}$$

Taking eq. (2.5) into eq. (2.2):

$$\sum_{k=1+IS_j}^{IE_j} (t_k - t_{k-1})\, v_k = \delta\phi_j \tag{2.6}$$

organized in a matrix form, finally leads to the expression

$$Bv = \delta\phi \tag{2.7}$$

In eq. (2.6) IE and IS corresponding to the acquisition time indexes are associated with the image pairs used for the interferogram generation and also we assume the master (IE) and slave (IS) images to be chronologically ordered, i.e. $IE_j > IS_j$, $\forall j = 1, \dots\dots\dots\dots, M$. In eq. (2.7), B is M x N matrix. When solving eq. (2.7) Singular Value Decomposition (SVD) is applied to matrix B, and the minimum-norm constraint for the velocity vector v is applied in final solution. To achieve the final solution ϕ an additional integration step is necessary.

In summary the SBAS approach had two key advantages:-

- It increases sampling rate by using all acquisitions included in the Small Baseline subsets.
- It preserves the capabilities of the system to provide spatially dense deformation maps, which being a key issue of conventional D-InSAR interferometry (Casu, et al., 2006).

2.3.3. CPT (Coherent Pixels Technique)

The Coherent Pixels Technique is one of the D-InSAR techniques able to obtain the full deformation pattern from a stack of interferograms (Mora, 2003). Here we will briefly explain how CPT calculates the deformation movement and atmospheric artefacts.

Once the differential interferograms are created and the pixels to be processed are selected, the deformation information from their phases are extracted. CPT algorithm is divided into two main blocks, the estimation of the linear differential phase i.e. linear velocity and DEM error and the estimation of the non-linear deformation where the estimation of the atmospheric artefacts is also done (Mora, 2003).

CPT algorithm assumes that the phase component linked to deformation ($\Delta\psi_{\mathrm{mov}}$) can be broken down into two new phase terms, one due to linear deformation ($\Delta\psi_{\mathrm{linear}}$) and another due to non-linear deformation ($\Delta\psi_{\mathrm{non-linear}}$).

Therefore,

$$\Delta\psi_{\mathrm{mov}} = \Delta\psi_{\mathrm{linear}} + \Delta\psi_{\mathrm{non-linear}} \quad (2.8)$$

$$= \left(\frac{4\pi}{\lambda}\right).\Delta v.\,T + \left(\frac{4\pi}{\lambda}\right).\Delta\rho_{\mathrm{non-linear}} \quad (2.9)$$

where λ is the radar wavelength, Δv is the velocity increment between pixels, T is the temporal seperation between both SAR acquisitions, and $\Delta\rho_{\mathrm{non-linear}}$ is the non-linear term of surface deformation. A brief description is given below (Mora, 2003):-

Estimation of the linear deformation:- In this case the selected pixels are related with a Delaunay triangulation that generates non-overlapped triangles. The selected pixels are the nodes related by the arcs of the triangulation. The basis for linear estimation is the adjustment of a linear model, which considers the linear velocity of deformation and the DEM error, to the available data (Mora, 2003). It is important to say that as no phase unwrapping is performed, CPT allows to recuperate the topography of the scene even when no DEM is employed.

Estimation of the non-linear deformation:- Once the linear term of deformation and DEM error have been estimated, the algorithm takes advantage of different behavior of the atmospheric artefacts with respect to the non-linear deformation in time and space to isolate their respective contributions to the phase (Mora, 2003). Spatial and temporal filtering is applied sequentially to separate both.

2.4. Empirical Mode Decomposition

Empirical Mode Decomposition (EMD) is an emerging method in signal processing proposed by Norden Huang (Huang, et al., 1998). EMD is the fundamental part of Hilbert Huang Transform (HHT). The biggest advantage of this method is that it is totally adaptive and data driven. This method is very much suitable for analyzing non-linear and non-stationary time series data. In contrast to other common transforms like Fourier Transform, HHT is more like an algorithm that can be applied to a data set, rather than a theoretical tool.

Using EMD algorithm any complicated data set can be decomposed into narrow band oscillatory components called Intrinsic Mode Functions (IMF). By definition, IMF's are the signals with following conditions:

- In the whole data set, the number of extremes (maxima & minima) and the number of zero crossings must either equal or must differ by a maximum of one.
- Each point, which is defined as mean value of envelopes defined by local maxima and local minima is zero.

The decomposition method used in EMD is called as "Sifting" process. This decomposition method operating in the time domain is adaptive and highly efficient. Since the decomposition is based on the local characteristic time scale of the data, it can be applied to non-linear and non-stationary processes. For sifting iteration cubic spline interpolation is preferred. Other interpolation techniques linear or polynomial tend to increase the required number of sifting iterations and also over-decomposes the signals by spreading out their components over adjacent nodes.

EMD has been widely used for data analysis such as image processing, bio-signals processing, seismic analysis and also for detecting mechanical faults of rotating machines.

The algorithm proceeds in the following steps Trnka and Hofreiter (2011):-

- Create upper envelope '$\mathrm{maxenv(t)}$' by local maxima and lower envelope '$\mathrm{minenv(t)}$' by local minima of data $y_1(t)$.
- Calculate the mean of upper envelope and lower envelope

$$m_1(t) = \frac{\mathrm{maxenv(t)+minenv(t)}}{2} \qquad (2.10)$$

- Subtract the mean from original data

$$h_1(t) = y_1(t) - m_1(t) \quad (2.11)$$

Where $m_1(t)$ is designated as mean and the difference between the data and $m_1(t)$ symbolizes the first component $h_1(t)$.

- Verify that $h_1(t)$ satisfies conditions for IMF's. Repeat steps 1 to 4 with $h_1(t)$ until it is an IMF.
- Get first IMF (after k iterations)

$$c_1(t) = h_{1(k-1)}(t) - m_1(t) \quad (2.12)$$

- Calculate first residue as

$$r_1(t) = y_1(t) - c_1(t) \quad (2.13)$$

- Repeat whole algorithm with $r_1(t), r_2(t), \ldots\ldots\ldots\ldots$ until residue is monotonic function.
- After N iterations $y_1(t)$ is decomposed and finally we obtain

$$y_1(t) = \sum_{i=1}^{N} c_i(t) + r(t) \quad (2.14)$$

3. STUDY AREA

The study area comprises of Jharia coalfield in the Indian state of Jharkhand. It is located in eastern India between 23˚40'40" to 23˚49'00" N latitude and 86˚10'00" to 86˚19'15" E longitude in the Survey of India toposheet 73 1/1, 2, 5 & 6 with an area of 450 km² approximately. Dhanbad is a major city located near the study area and is well known as the "Coal Capital of India". It is bounded by Dumra, Katrasgarh townships in the north, by Katri river in the east, by Chandrapur township in the West and extends little south of Damodar river in the south.

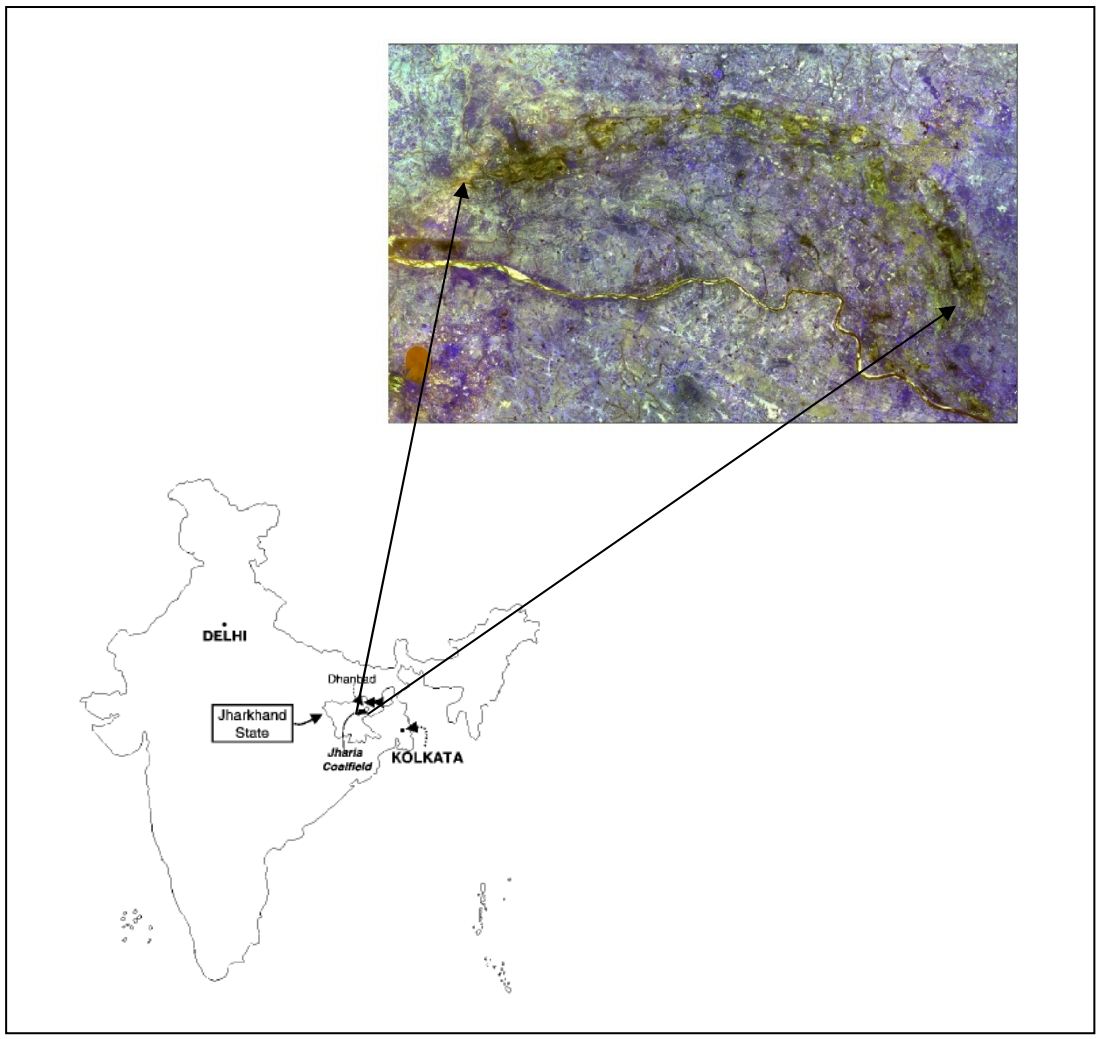

Figure 3.1: Location of the study area

3.1. Attributes of the study area

- Jharia coalfield consists of mainly sedimentary rocks.
- The coalfield lies in Damodar river valley, and covers about 240 square km and produces bituminous coal suitable for coke making (Masto, et al., 2011).
- The coalfield has more than 40 workable coal seams out of which the upper seams have coals of superior quality and this quality deteriorates with the seams at deeper horizons.
- There are many underground mines in the coalfield, but major mining activity is done by opencast mining method.
- Dense population over affected areas and in underground mining areas approximates to 1.1 million.
- The coalfield is characterized by gently undulating to rolling topography with an overall slope towards east-southeast (Singh, 2010).
- The coalfield having an area of about 450 km² belongs to Gondwana group of Permian age and has Talchir, Barakar, Barren Measures and Raniganj Formations.
- The major coal-bearing formation in Jharia coalfield, the Barakar Formation of Early Permian age in the northern part of the coalfield is severely fire affected (Chatterjee, et al., 2007).

3.2. Geology of the study area

3.2.1. Coal reserve

As on 01/04/2007 geological coal reserves of Jharia coalfield within the leasehold of BCCL (Bharat Coking Coal Limited) is upto a depth of 1200m. The total surface area of BCCL affected due to fire had been assessed to be 8.9 km² in 1995 against the earlier area of about 17 km² at the time of nationalization. The quantum of coal burnt as per earlier assessment is 37 million tones and total reserves are about 17,077 million tones.

3.2.2. Mining history and present status

India has a long history of commercial coal mining covering nearly 220 years starting from 1774 by M/s Sumner and Heatly of East India Company in the Raniganj coalfield along the Western bank of river Damodar. However, for about a century the growth of Indian coal mining remained sluggish but the introduction of steam locomotives in 1853 gave a fillip to it.

Coal mining was started in Jharia coalfield in the early 1890's (Singh, et al., 2010). Coal is the primary source of energy in India. Mining in this coalfield was started about 100 years ago and is still continuing. It was proven that the crescent shaped basin of the coalfield has approximately 1 billion tons of coal reserves (Singh, et al., 2010). BCCL is the primary mining agency in this area and it supplies about 40% of nation's coking coal.

The present status of Jharia coalfield appears difficult to plan for scientific mining due to various constraints such as due to the presence of fires, buildings, and other surface properties. On a rough estimate about 75% of the total coal reserves in the coalfield are still available and there is a need for long-term planning <http://www.oocities.org/vibhaskumar/jharia_ncs1.html>. It is anticipated that if suitable measures are not taken in time the coalfield in about 30 years time may present a deserted and bleak look <http://www.oocities.org/vibhaskumar/jharia_ncs1.html>.

3.3. Scientific importance of the study area

Jharia coalfield is one of the best for mining because it had several thick coal seams which were at shallow depths beneath the surface. The uniqueness of this coalfield is not only in its geologic formation but also in land degradation, mine fires and environmental pollution. It is considered to be one of the world's most degraded coalfields (Singh, et al., 2010). Land subsidence is one of the major causes of land degradation around this coalfield.

It is evident that different types of scatterers are found in this study area. Buildings and other urban features around Dhanbad city act as permanent scatterers. The water bodies like Damodar River in the south of the study area causes specular reflection to the RADAR signal. The terrain is continuously changing with time due to mining activities. Interferometric pairs with low temporal baselines would be feasible to get accurate deformation measurements.

4. DATA USED AND METHODOLOGY

4.1. Materials used in the study

4.1.1. ALOS PALSAR data

ALOS (Advanced Land Observing Satellite) was successfully launched on 24th January, 2006 by JAXA (Japan Aerospace Exploration Agency) and PALSAR (Phased Array type L-band Synthetic Aperture Radar) is the sensor which is carried by ALOS. PALSAR can operate at four primary modes with diverse polarizations and offnadir angles: (a) high-resolution single-polarization (FBS) mode, (b) high-resolution dual-polarization (FBD) mode, (c) fully-polarimetric (PLR) mode, and (d) ScanSAR mode.

ALOS orbits at an altitude of 691.65 km (at the equator) with 46-days repeat cycle. The center frequency of PALSAR is 1270 MHz, resulting in a wavelength of 23.62 cm and incidence angle 34.3˚.

Table 4.1: ALOS PALSAR data specifications

Sl. no.	Orbit	Path	Date of Pass	Mode	Polarization	Frame	Node
1	05421	510	30/01/2007	FBS	HH	460	Ascending
2	10118	510	18/12/2007	FBS	HH	460	Ascending
3	10789	510	02/02/2008	FBS	HH	460	Ascending
4	11460	510	19/03/2008	FBS	HH	460	Ascending
5	15486	510	20/12/2008	FBS	HH	460	Ascending
6	20854	510	23/12/2009	FBS	HH	460	Ascending
7	21525	510	07/02/2010	FBS	HH	460	Ascending
8	26222	510	26/12/2010	FBS	HH	460	Ascending

4.1.2. Digital Elevation Model (DEM)

Merged SRTM (Shuttle Radar Topographic Mission) and CARTOSAT DEM (2006 and 2011) of 25m and 10m spatial resolution respectively are used in the study with projection UTM (Universal Transverse Mercator), zone 45N and datum WGS-84. The vertical accuracy is 8m and horizontal accuracy is 15m.

4.1.3. CARTOSAT image

Geocoded CARTOSAT-1 image of resolution 2.5m was also used in the study for map composition.

4.2. Methodology

The methodology adopted in this research work is illustrated below:

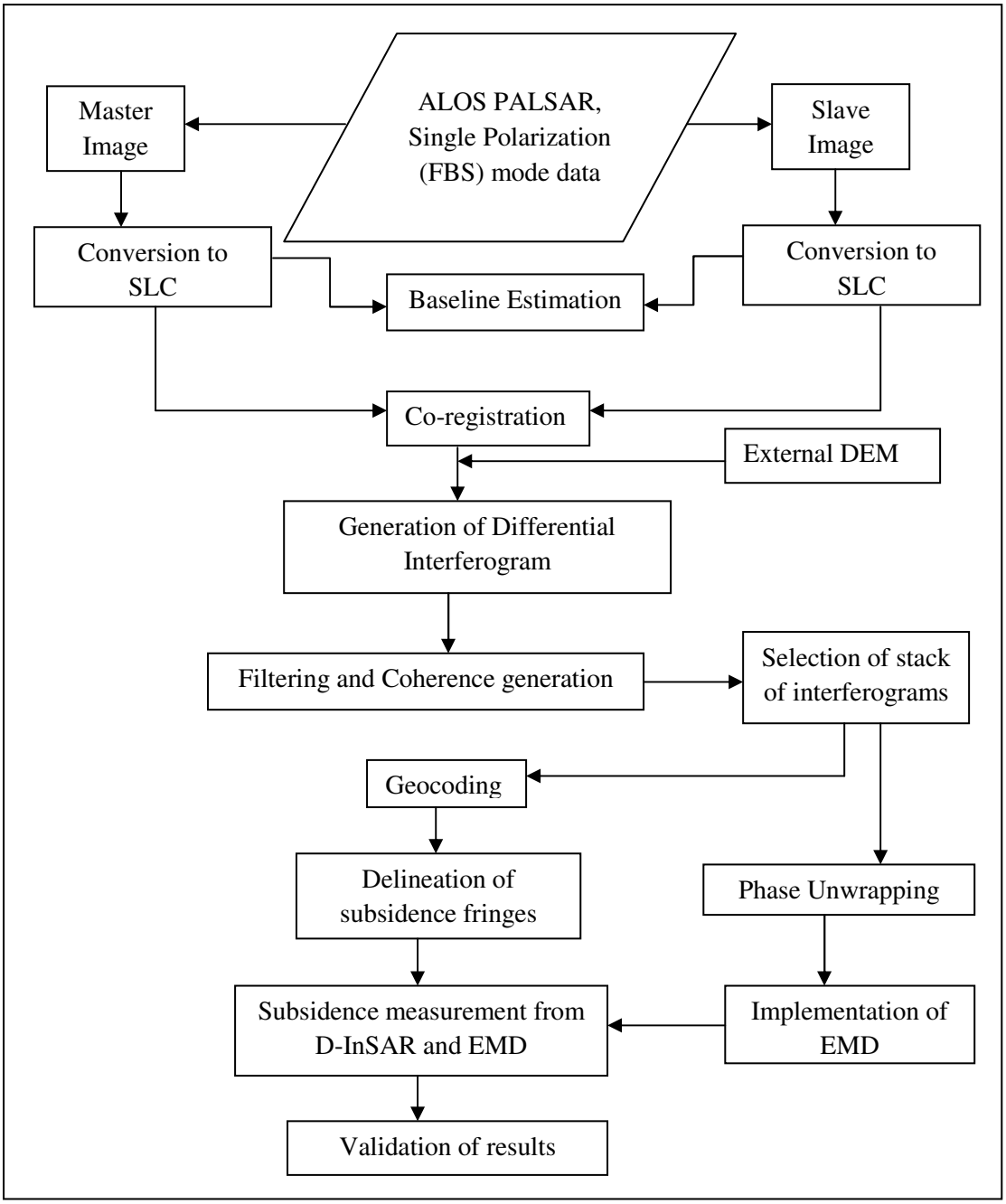

Figure 4.1: Flow diagram of the methodology adopted

4.2.1. Pre-processing of ALOS PALSAR data

Firstly from raw data by observing date of pass master image and slave image is created. Then the raw files are imported into SARscape and converted into SLC (Single Look Complex) format. Since it is difficult to interpret the features in this format so multilooking is done for interpreting the actual boundary. After that using top left and bottom right co-ordinates of multilooked image, SLC images are subsetted. Then all those subset images are used for baseline estimation and interferogram generation.

4.2.2. D-InSAR processing

The steps for D-InSAR processing are shown below:

- **Baseline estimation**

This step enables to obtain information about the baseline values and other orbital parameters related to the input pair. The generation of an interferogram is only possible when the ground reflectivity acquired with at least two antennae overlap (SARscape, 2013). When the perpendicular component of the baseline B_n increases beyond a certain limit known as critical baseline, no phase information is preserved, coherence is lost and interferometry is not possible (SARscape, 2013). The critical normal baseline $B_{n\sigma}$ can be calculated as:

$$B_{n\sigma} = \frac{\lambda R \tan\theta}{2R_r} \qquad (4.1)$$

where λ is the wavelength, R is the range distance, R_r is the pixel spacing in range and θ is the incidence angle (SARscape, 2013).

The sensibility to detect height variations is inversely proportional to 2π ambiguity height (SARscape, 2013). The bigger the ambiguity height the worse is the capability to detect small elevation changes (SARscape, 2013). The 2π ambiguity height AH can be calculated as:

$$AH = \frac{\lambda R \sin\theta}{4\pi B_n} \qquad (4.2)$$

- **Interferogram generation**

The distance difference between a point on the earth and the sensor position on the two acquisitions at different revisit times can be measured by the phase difference ϕ between two complex SAR images (SARscape, 2013). This is performed by multiplying one image by the complex conjugate of the other one where an interferogram is formed (SARscape, 2013).

An interferogram is an image representation of pixel-by-pixel phase difference between two SAR images. The phase of the interferogram contains fringes that trace the topography or displacement like contour lines (SARscape, 2013).

The interferometric phase is expressed as:

$$\text{Phase} = \text{ATAN}[\text{Imag(I)}/\text{Real(I)}] \quad (4.3)$$

where Imag(I) and Real(I) are the imaginary and real parts of the interferogram (SARscape, 2013).

- **Interferogram flattening**

In this step the reference DEM is given as input which removes topography from the interferogram. The previously generated interferogram is split into synthetic phase and residual phase (differential phase). Then the input DEM is re-projected onto the master SAR geometry and is re-generated as slant range DEM. The DEM mentioned in section 4.1.2. was used to generate differential interferograms which contains subsidence fringes.

- **Adaptive filter and coherence generation**

The filtering of the flattened interferogram enables to generate an output product with reduced phase noise (SARscape, 2013). The sources of phase noise in the interferogram are baseline decorrelation and temporal decorrelation.

Interferometric coherence which is an indicator of the phase quality is also generated (SARscape, 2013). The interferometric coherence γ calculated from two input SAR images (S_1) and (S_2) is defined as (SARscape, 2013):

$$\gamma = \frac{|\sum S_1(x) \cdot S_2(x)^*|}{\sqrt{\Sigma|S_1(x)|^2 \cdot \Sigma|S_2(x)|^2}} \quad (4.4)$$

where $S_1(x)$ is master image, $S_2(x)$ is slave image and $S_2(x)^*$ is the complex conjugate of slave image.

The coherence image values range in between 0 and 1. Value 1 indicates areas with high coherence and value 0 indicates areas with low coherence. The estimated coherence which ranges between 0 and1 is function of systematic spatial de-correlation (i.e. the additive noise) and temporal de-correlation between master and slave acquisitions (SARscape, 2013).

Filtering is essential to minimize the phase noise and retrieve the surface information which is present in the phase of the interferogram (Chen, et al., 2012). In this work, Boxcar filter was applied to identify the subsidence fringes.

Table 4.2: Details of interferogram pairs

Sl. No.	Master Orbit - Slave Orbit	Date of Pass (yyyy/mm/dd)		$B_{\perp}$ (m) (Critical = 13043.496m) (Altitude of ambiguity, Ha	Δt (days)	Season	Doppler shift (Hz) (Critical = 2159.827 Hz)	Average scene Coherence
		Master Scene	Slave Scene					
1	05421 - 10118	1/30/2007	12/18/2007	1319.362 (48.606)	322	Jan-Dec	-8.6	0.072 ± 0.052
2	05421 - 10789	1/30/2007	2/2/2008	1849.714 (34.670)	368	Jan-Feb	-10.736	0.056 ± 0.038
3	05421 - 11460	1/30/2007	3/19/2008	1675.414 (38.276)	414	Jan-Mar	-15.595	0.061 ± 0.041
4	05421 - 15486	1/30/2007	12/20/2008	822.452 (77.973)	690	Jan-Dec	0.266	0.088 ± 0.065
5	05421 - 20854	1/30/2007	12/23/2009	770.183 (83.264)	1058	Jan-Dec	9.287	0.084 ± 0.063
6	05421 - 21525	1/30/2007	2/7/2010	1159.434 (55.310)	1104	Jan-Feb	-7.132	0.069 ± 0.050
7	05421 - 26222	1/30/2007	12/26/2010	1993.667 (32.166)	1426	Jan-Dec	-0.143	0.045 ± 0.030
8	10118 - 10789	12/18/2007	2/2/2008	534.476 (119.621)	46	Dec-Feb	-2.136	0.370 ± 0.108
9	10118 - 11460	12/18/2007	3/19/2008	356.375 (179.403)	92	Dec-Mar	-6.995	0.325 ± 0.125
10	10118 - 15486	12/18/2007	12/20/2008	2127.207 (30.056)	368	Dec-Dec	8.867	0.042 ± 0.029
11	10118 - 20854	12/18/2007	12/23/2009	582.232 (109.809)	736	Dec-Dec	17.887	0.105 ± 0.078
12	10118 - 21525	12/18/2007	2/7/2010	172.556 (370.514)	782	Dec-Feb	1.468	0.137 ± 0.099
13	10118 - 26222	12/18/2007	12/26/2010	682.787 (93.638)	1104	Dec-Dec	8.457	0.086 ± 0.066
14	10789 - 11460	2/2/2008	3/19/2008	180.531 (353.691)	46	Feb-Mar	-4.859	0.453 ± 0.138
15	10789 - 15486	2/2/2008	12/20/2008	2656.366 (24.037)	322	Feb-Dec	11.002	0.015 ± 0.014
16	10789 - 20854	2/2/2008	12/23/2009	1112.661 (57.387)	690	Feb-Dec	20.023	0.072 ± 0.054
17	10789 - 21525	2/2/2008	2/7/2010	693.173 (92.116)	736	Feb-Feb	3.604	0.098 ± 0.072
18	10789 - 26222	2/2/2008	12/26/2010	279.099 (228.780)	1058	Feb-Dec	10.593	0.115 ± 0.089
19	11460 - 15486	3/19/2008	12/20/2008	2483.522 (25.718)	276	Mar-Dec	15.861	0.022 ± 0.018
20	11460 - 20854	3/19/2008	12/23/2009	930.540 (68.638)	644	Mar-Dec	24.881	0.077 ± 0.057
21	11460 - 21525	3/19/2008	2/7/2010	521.041 (122.582)	690	Mar-Feb	8.463	0.110 ± 0.079
22	11460 - 26222	3/19/2008	12/26/2010	358.043 (178.387)	1012	Mar-Dec	15.452	0.113 ± 0.086
23	15486 - 20854	12/20/2008	12/23/2009	1591.344 (40.356)	368	Dec-Dec	9.02	0.066 ± 0.046
24	15486 - 21525	12/20/2008	2/7/2010	1959.582 (32.772)	414	Dec-Feb	-7.398	0.050 ± 0.034
25	15486 - 26222	12/20/2008	12/26/2010	2792.821 (22.995)	736	Dec-Dec	-0.409	0.012 ± 0.011
26	20854 - 21525	12/23/2009	2/7/2010	482.554 (132.613)	46	Dec-Feb	-16.418	0.440 ± 0.121
27	20854 - 26222	12/23/2009	12/26/2010	1216.736 (52.594)	368	Dec-Dec	-9.429	0.073 ± 0.053
28	21525 - 26222	2/7/2010	12/26/2010	854.863 (74.816)	322	Feb-Dec	6.989	0.103 ± 0.071

All the 10 highlighted pairs of the above table are used in further processing, because these are the interferograms in which the fringes are overlapped.

- **Phase unwrapping**

The phase of the interferogram can only be modulo 2π; hence anytime the phase change becomes larger than 2π, the phase starts again and the cycle repeats itself (SARscape, 2013). Phase unwrapping is the process for resolving this 2π ambiguity. In this work phase unwrapping is performed by minimum cost flow algorithm with coherence threshold 0.1.

4.2.3. Implementation of EMD

EMD is applied on these stack of unwrapped interferograms at each pixel where all subsidence fringes are present, and the reconstructed D-InSAR time series was used for further analysis.

The trend analysis was carried out using statistical trend test approach, because statistical trend tests provide better way to describe trends in long time series than linear regression. In this work the primary testing of trends in residue obtained by EMD of D-InSAR time series

was done by Mann-Kendall test and Sen's slope estimator was used to find the slope of the trend.

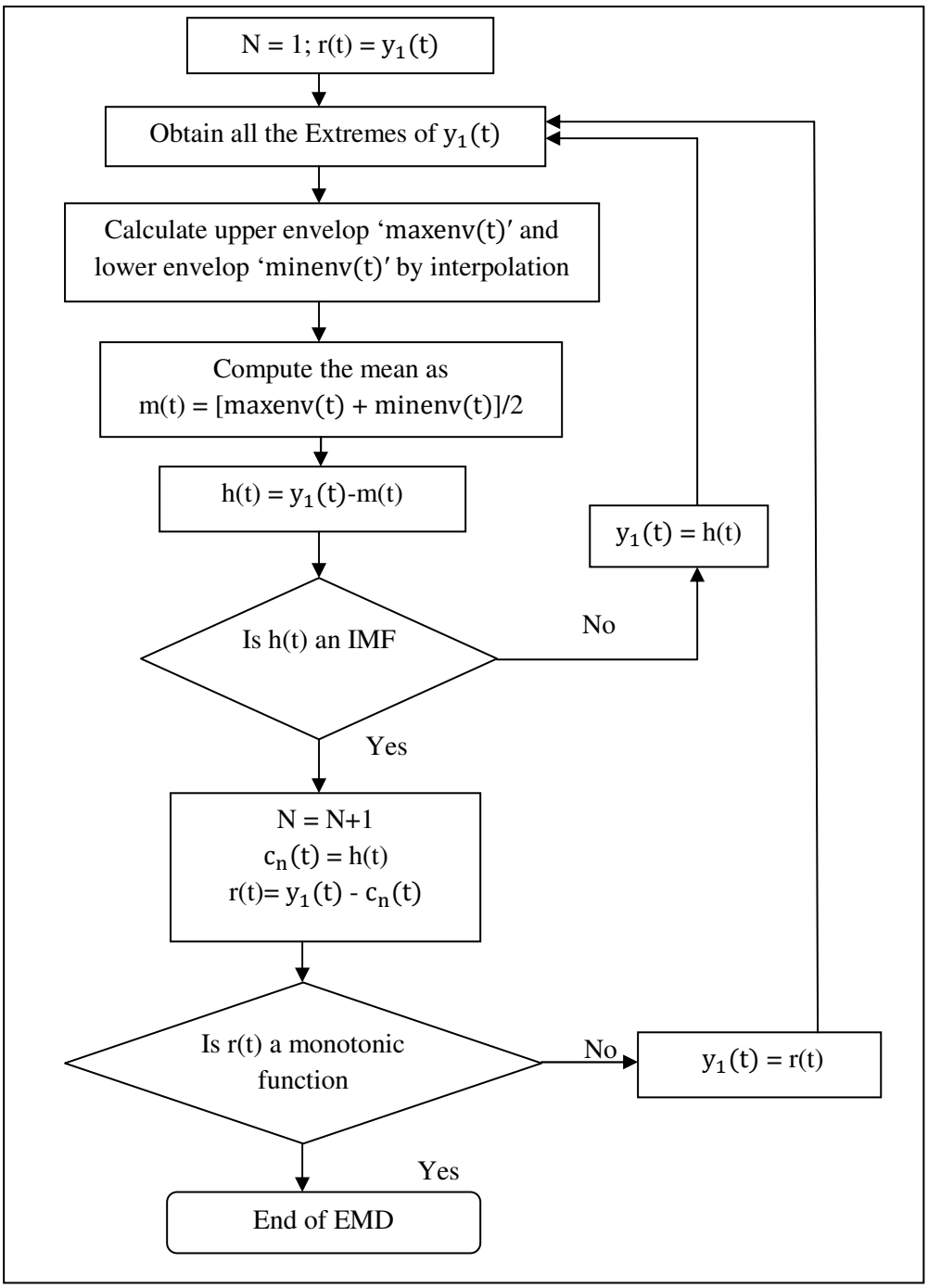

Figure 4.2: Flow diagram of EMD algorithm

4.2.4. Validation of subsidence measurements

All the 10 highlighted differential interferograms are geocoded and the basin boundary (Jharia basin boundary) is overlayed on those geocoded images for the identification of subsidence fringes. Subsidence rate is calculated through these identified fringes from each differential interferogram and then weighted subsidence rate is calculated for each overlapped fringes. After that subsidence generated from D-InSAR and EMD are validated with respect to spatial extent and field evidences.

In a differential interferogram, each fringe or a complete phase cycle (2π radian phase difference) represents $\lambda/2$ land displacement along the radar line-of-sight, where λ is wavelength of the radar pulse (Chatterjee, et al., 2010).

In case of ALOS PALSAR $2\pi = \lambda/2 = 23.62/2 = 11.81$cm

$$\text{LOS deformation} = \frac{n}{N} \times 11.81 \qquad (4.5)$$

where n is the number of colours in the fringe and N is total number of colours considered (in this case 8)

Therefore,

$$\text{Subsidence rate} = \frac{\text{LOS deformation}}{\Delta t} \times D \qquad (4.6)$$

where Δt is temporal baseline in days and D is total number of days in a year.

5. RESULTS AND DISCUSSION

5.1. D-InSAR processing results

Multiple ALOS PALSAR data pairs with suitable spatial baselines were processed to identify the subsiding areas. Some of the pairs were not found appropriate for D-InSAR applications due to high temporal decorrelation and changes in the topography due to opencast mining activities. However, some D-InSAR pairs are found to show well-defined fringes in filtered differential interferograms. It is observed that in all 10 highlighted pairs in table 4.2 the fringes are seen in the interferograms which denote continuous land subsidence and their rates of subsidence have been calculated using the formula in section (4.2.4).

One of the limitations of selecting the suitable pairs is the interferometric phase noise caused by the decorrelation between the two acquisitions. The level of phase noise depends upon both spatial and temporal baselines of the two acquisitions as well as the imaging resolution.

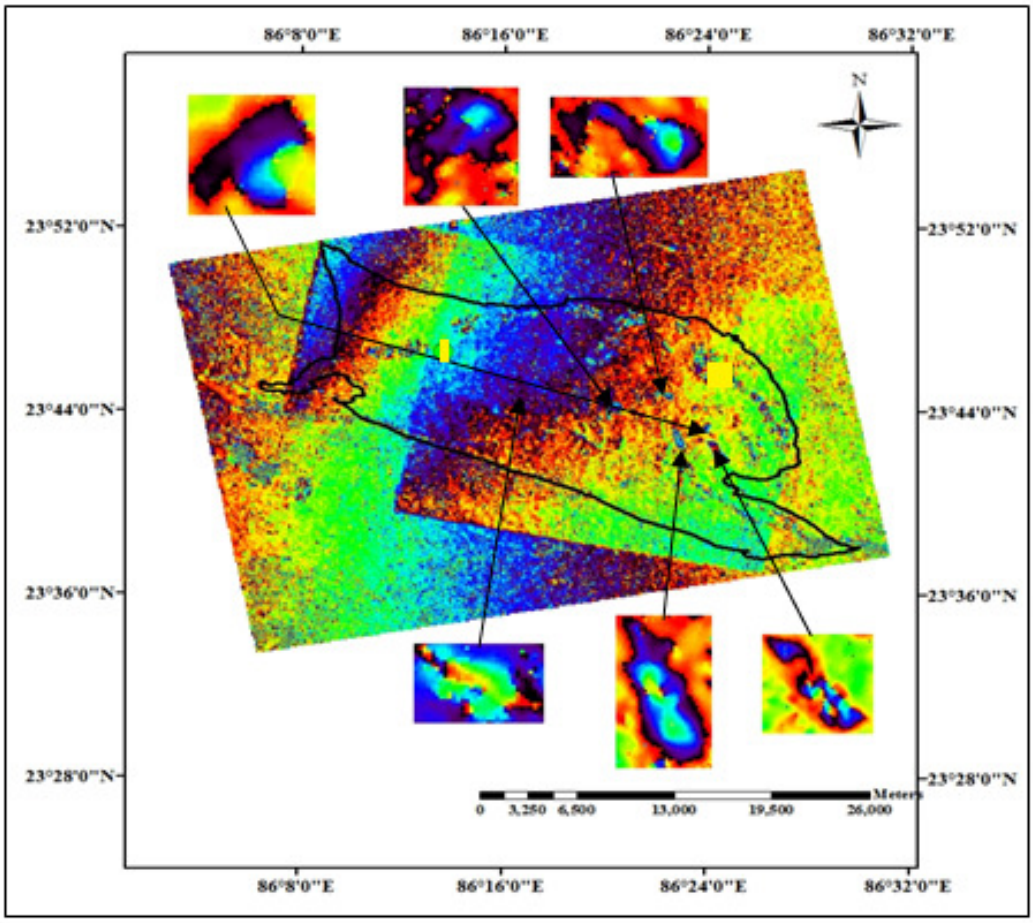

Figure 5.1: Differential interferogram of the pair 10118-20854 with subsidence fringes

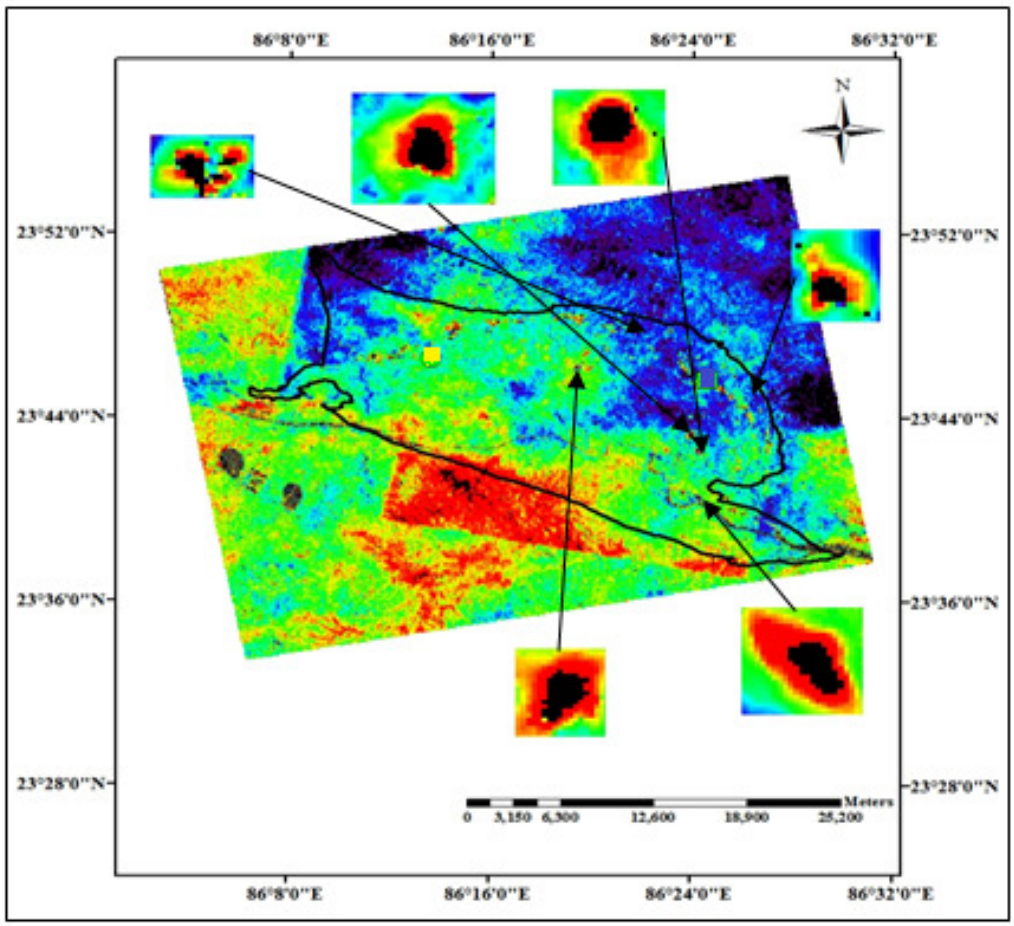

Figure 5.2: Differential interferogram of the pair 10118-11460 with subsidence fringes

It is clearly observed from the above figures that most of the subsidence fringes were in the eastern parts of the coalfield, but some are in the south-eastern and north-western part of the study area. Fringes are seen in the area affected by extensive underground coal mining. Fringes were checked in the field and subsidence areas were confirmed.

The fringes observed in these interferograms were overlayed on CARTOSAT image for localization of subsidence areas (Figure 5.3). LOS deformation and subsidence rate for each of the fringes was calculated and then finally the weighted average of subsidence rate was calculated for continually subsiding areas, i.e. where overlapping fringes were seen in multiple interferograms.

Subsidence fringe areas were extracted from each of the interferograms and combined together to obtain the total subsidence affected areas.

The maximum subsidence rate calculated through D-InSAR processing is 35.235cm/year and minimum is 17.62cm/year.

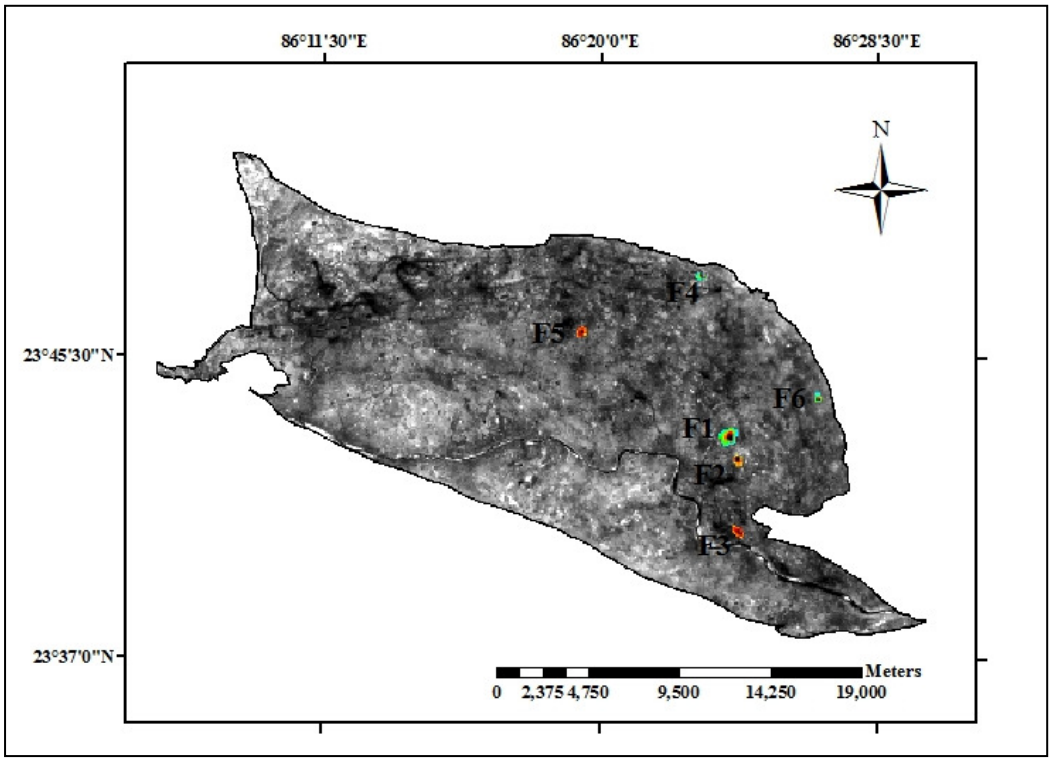

Figure 5.3: Map showing subsidence fringes placed over CARTOSAT image

Table 5.1: Affected surface area of each fringe and subsidence rates calculated from D-InSAR

Fringe ID	Fringe Area (m^2)	Subsidence Rate (cm/year)
F1	574515.629077	28.492
F2	146766.977003	17.62
F3	151932.160426	23.492
F4	157541.189112	35.235
F5	138688.020672	23.492
F6	123675.272867	30.363

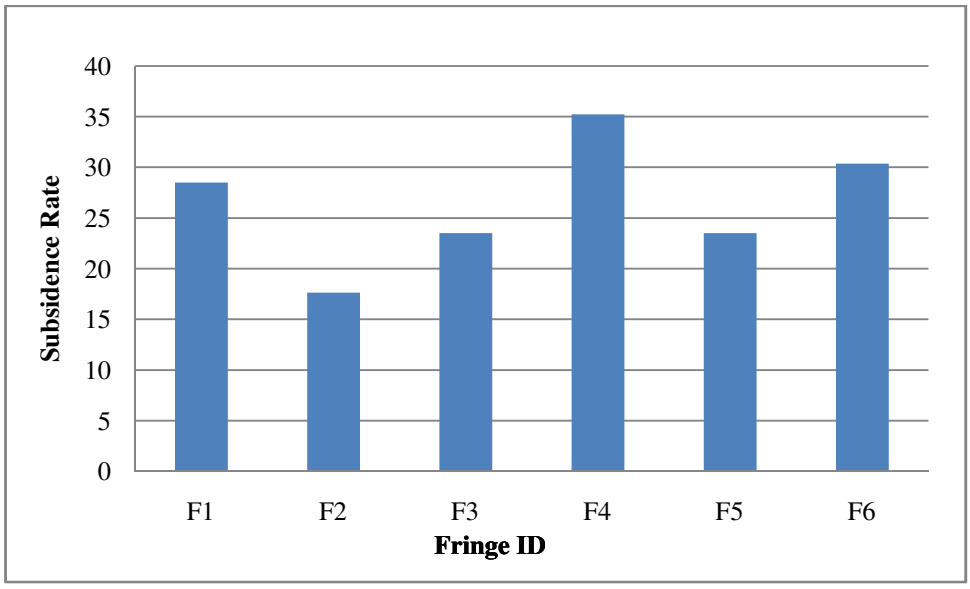

Figure 5.4: Subsidence rate of fringe areas obtained from D-InSAR

5.2. EMD results

EMD was used for deformation modeling i.e. separation of linear and non-linear deformation. It was applied on stack of unwrapped interferograms at each pixel where subsidence fringes are present. EMD basically decomposes an image into simpler monocomponent signals called IMF and residue which can be either mean trend or constant. In this work, IMF corresponds to non-linear deformation and residue corresponds to linear deformation. The significance of non-linear deformation is that it represents a particular trend, so for each fringe area statistics of IMF and residue was calculated. Subsidence estimated by EMD and that estimated through D-InSAR are compared and shown in table below.

Table 5.2: Comparison of subsidence calculated by D-InSAR and EMD

Fringe ID	Subsidence				
	D-InSAR (cm/year)	EMD			
		Residue (cm)		IMF (cm)	
		Min-Max	Mean ± Std.Dev.	Min-Max	Mean ± Std.Dev.
F1	28.492	12.72-25.45	19.88 ± 5.43	12.79-47.39	36.94 ± 16.19
F2	17.62	0.17-0.86	0.55 ± 0.23	14.31-37.11	23.32 ± 10.51
F3	23.492	2.85-4.56	3.71 ± 1.21	18.7-24.07	24.39 ± 6.8
F4	35.235	4.23-12.69	8.46 ± 3.6	29.02-38.6	37.8 ± 30.37
F5	23.492	4.43-8.87	20.07 ± 0.92	16.59-25.65	28.56 ± 21.71
F6	30.363	10.29-27.46	18.88 ± 12.1	18.08-43.37	35.46 ± 28.49

In the above table both the results obtained from D-InSAR and EMD are representing subsidence. From D-InSAR subsidence rate is calculated, whereas from EMD trends of subsidence was calculated which is equivalent to subsidence rate.

It is clearly observed from the results that all the parameters of Residue and IMF are following a particular trend, i.e. linear deformation is less than non-linear deformation for all subsidence fringes. Also it can be observed that for all fringes the range of subsidence obtained from EMD are within that obtained from D-InSAR, but the subsidence calculated from EMD is higher than that calculated from D-InSAR.

5.3. Validation

From the differential interferograms in (Figure 5.1 and Figure 5.2) the subsidence fringes were observed in Dubrajpur, Baradubhi, Jamadoba, Digwadih, Bhowrah and Jharia respectively. All these fringes were checked in the field and also we came to know from BCCL officers that subsidence is occurring in these places due to underground coal mining activities since 2008 and also in places like Lodna, Bararee, Sijua, Ekra Pool and Digwadih subsidence was occurring due to coal fires. Recently in 2012 we have seen that in Bastacola subsidence is taking place due to underground mining activities.

Subsidence rate statistics of Bastacola area are shown below:-

Minimum subsidence rate observed:	18.2 cm/year
Maximum subsidence rate observed:	45.4 cm/year
Mean subsidence rate of 73 pillars:	111.853 cm/year

Leveling based rate measured during active mining phase gives high rate, but D-InSAR pairs do not overlap with leveling measurements at Bastacola.

6. CONCLUSIONS AND RECOMMENDATIONS

6.1. Conclusions

D-InSAR is widely used tool for measuring topographic profile and spatially continuous surface deformation. A good quality DEM was used for removal of topography and identify displacement phase which is the primary aim of D-InSAR. In this work EMD was used, since the main focus is on modeling of deformation history. EMD is totally adaptive and data driven approach and is suitable for analyzing non-linear and non-stationary time series data.

In spite of the wide application of InSAR and D-InSAR, there are number of limitations and sources of error that invoke special consideration in applications of D-InSAR. The general limitations can be listed as follows:

- Poor temporal resolution i.e. limited satellite coverage.
- Decorrelation of images.
- Orbital, atmospheric and topographic errors.
- Low coherence.
- Phase errors due to processing.
- D-InSAR processing software has a high level of complexity and relatively requires long time to understand.

Q.1) How far L-band data is suitable for detecting surface deformation areas?

Ans:) It is seen that L-band data, specially ALOS PALSAR can be used successfully for delineating moderate to rapidly surface deformation areas as compared to any optical remote sensing data. From the differential interferograms, most of the subsidence fringes were occurred in Dubrajpur, Baradubhi, Jamadoba, Digwadih, Bhowrah and Jharia respectively. So this proves that L-band data is more advantageous than any other data (whether microwave/optical) for detecting coal mining induced subsidence.

Q.2) How far EMD is suitable for deciphering deformation history?

Ans:) The purpose of identifying linear and non-linear deformation is for modeling of deformation time series – testing of trends. This modeling can also be done by some other advanced D-InSAR techniques such as CPT, SBAS but they requires large number of datasets. EMD overcomes from this limitation of datasets and also it is suitable for analyzing non-linear and non-stationary time series data. The results in table 5.2 indicates that EMD is very much suitable for deciphering deformation history.

6.2. Recommendations

The present study aims at modeling of deformation time series by Empirical Mode Decomposition technique, but land subsidence modeling can also be done by some advanced D-InSAR techniques such as PS (Persistent Scatterers), SBAS (Small Baseline Subset) and CPT (Coherent Pixels Technique). Deformation modeling through EMD is similar to SBAS approach, but SBAS cannot be applied in this work because of limited number of datasets. So, if the study could be performed by using these techniques especially SBAS then the results obtained from EMD could be analyzed and compared. Also non-availability of sufficient number of good quality D-InSAR pairs limits land subsidence modeling study on a multi-temporal basis. Therefore it is recommended that in future for performing this kind of work number of datasets should be more, at least 35 pairs of images. This could enhance and improve the modeling approach and also any of the D-InSAR techniques can be applied.

REFERENCES

I. H. Woodhouse, "Introduction to Microwave Remote Sensing", *CRC Press*, 2006.

R. Burgmann, E. J. Fielding and P. A. Rosen "Synthetic Aperture Radar Interferometry to Measure Earth's Surface Topography and its Deformation," *Annual Review Earth Planet Science*, pp. 169-209, 2000.

R. F. Hanssen, "Radar Interferometry: Data Interpretation and Error Analysis", *Springer*, 2001.

P. A. Rosen, E. Rodriguez, F. K. Li, I. R. Joughin, R. M. Goldstein, S. Hensley and S. N. Madsen "Synthetic aperture radar interferometry," *Proceedings of IEEE*, vol. 88, No.3, pp.333-382, 2000.

A. K. Gabriel, H. A. Zebker and R. M. Goldstein, "Mapping small elevation changes over large areas: Differential Radar Interferometry", *J.Geophys.Res*., vol.94, no. B7, pp.9183-9191, 1989.

R. S. Chatterjee, B. Fruneau, J. P. Rudant, P. S. Roy, P. L. Frison, R. C. Lakhera, V. K. Dadhwal and R. Saha, "Subsidence of Kolkata (Calcutta) city, India during the 1990s as observed from space by Differential Synthetic Aperture Radar Interferometry (D-InSAR) technique," *Remote Sensing of Environment*, vol. 102, pp. 176-185, 2006.

R. D. Lokhande, Amar Prakash and K. B. Singh, "Surface Ground Deformation in Jharia and Raniganj coalfields over old mine workings," *Indian Journal Environmental Protection*, Vol. 29, No.4 pp. 289-292, 2009.

N.C.Saxena, "Subsidence Management in Jharia Coalfield, India — A Concept", *Proceedings of the Fourth International Symposium on Land Subsidence*, IAHS Publ. no. 200, pp. 181-184, 1991.

S. C. Bannerjee, "Spontaneous combustion of coal and mine fire", *Oxford and IBH Publishing Co. PVT. Ltd*., pp 125-139, 1985.

Antonio M. Ruiz, Antonio J. Gil, Jesus Galindo-Zaldivar, Joaquim J. Sousa, Luisa Bastos, Ramon F. Hanssen and Zbigniew Perski, "PS-InSAR measurement of Ground Subsidence in Granada area (Betic Cordillera, Spain)", *13th FIG Symposium on Deformation Measurement and Analysis*, May 12-15, 2008.

A. Ferretti, C. Prati and F. Rocca, "Permanent Scatterers in SAR Interferometry", *IGARSS Proceeding*, Hamburg, Germany, pp. 1528-1530, 1999.

A. Ferretti, C. Prati and F. Rocca, "Nonlinear Subsidence Rate Estimation using Permanent Scatterers in Differential Interferometry", *IEEE TGARS*, Vol. 38, No.5, pp.2202-2212 , September 2000.

A. Ferretti, C. Prati and F. Rocca, "Permanent Scatterers in SAR Interferometry", *IEEE TGARS*, Vol. 39, No.1, pp.8-20, January 2001.

P. Berardino, G. Fornaro, R. Lanari and E. Sansosti, "A new algorithm for surface deformation monitoring based on small baseline differential interferograms," *IEEE Transactions on Geosciences and Remote Sensing*, Vol.40, No. 11, 2375-2383, 2002.

P. Tizzani, P. Berardino, F. Casu, P. Euillades, M. Manzo, G. P. Ricciardi, G. Zeni and R. Lanari, "Surface deformation of Long Valley Caldera and Mono Basin, California, investigated with the SBAS-InSAR approach", *Remote Sensing of Environment* 108 : pp.277-289, 2007.

F. Casu, M. Manzo, R. Lanari. "A quantitative assessment of the SBAS algorithm performance for surface deformation retrieval from D-InSAR data", *Remote Sensing of Environment* 102, pp. 195-210, 2006.

O. Mora, "Linear and non-linear terrain deformation maps from a reduced set of interferometric SAR images", *IEEE Transactions on Geosciences and Remote Sensing*, Vol. 41, pp.2243-2253, 2003.

N. E. Huang, Z. Shen, S. R. Long, M. L. Wu, H. H. Shih, Q. Zheng, N. C. Yen, C. C. Tung and H. H. Liu, "The empirical mode decomposition and Hilbert spectrum for non-linear and non-stationary time series analysis", *Proc. Roy. Soc London A*, Vol.454, pp.903-995, 1998.

P. Trnka and M. Hofreiter "Empirical Mode Decomposition in Real-Time" 18th *International Conference on Process Control* June 14-17, 2011, Tatranska Lomnica, Slovakia.

R. S. Chatterjee, Md. Wahiduzzaman, R. C. Lakhera, V. K. Dadhwal and E. V. R. Raju, "Dynamics of coal fire in Jharia Coalfield, Jharkhand, India during the 1990s as observed from space", *Current Science*, Vol.92, No.1, 10 January, 2007.

R. E. Masto, A. K. Sinha, A. Sinha, D. Mohanty, J. George, L. C. Ram, N. K. Srivastava, R. C. Tripathi, S. K. Jha, S. K. Verma and V. A. Selvi, "Rare Earth Elements in Soils of Jharia Coal Field" , *World Academy of Science, Engineering and* Technology, Vol.52, 2011.

G. Singh, " Environmental Impact Assessment of Mining Projects", *Proceedings of 3rd Int. Conf. on Southeast Asian Natural Resources and Environmental Management* Jointly Organized by School of Science and Technology, UMS and Science & Technology Unit, Sabah, Malaysia during August 3-5, 2010.

G. Singh, B. Paul, E. V. R. Raju, M. K. Jain and R. D. Gupta, "Clusterization of mines for obtaining comprehensive environmental clearance: A case study of BCCL Lease hold areas", *Journal of Indian School of Mines*, special vol., pp.13-20, 2010.

SARscape, "Synthetic Aperture Radar and SARscape," Feb-2013.

K. S. Chen, C. F. Chao, C. T. Wang and J. S. Lee, "Refined filtering of interferometric phase from InSAR data," in *Geosciences and Remote Sensing Symposium (IGARSS)*, 2012 *IEEE International*, pp.1821-1824, July 2012.

R. S. Chatterjee, Moh. Fifik Syafiudin and Hasanuddin Z. Abidin, "Land Subsidence scenario in Bandung city and surrounding areas of Bandung basin, Indonesia by Space

borne Differential Interferometric Synthetic Aperture Radar (D-InSAR) technique", *Proceedings PIT IAGI LOMBOK 39th IAGI Annual Convention and Exhibition* , 2010.

Websites

- http://www.infraline.com.
- http://en.wikipedia.org/wiki/Hilbert_Huang_transform.
- http://www.oocities.org/vibhaskumar/jharia_ncs1.html.

APPENDIX

Field Photographs

Coal fires near Bararee

Leveling of subsidence pillars in Mahespur

Leveling of subsidence pillars in Bastacola

Subsidence occurred in Bastacola area

Cracks occurred in Mahespur